Electroproduction of K^+ mesons along the virtual-photon direction*

C. J. Bebek, C. N. Brown,† P. Bucksbaum, M. Herzlinger, S. D. Holmes,
C. A. Lichtenstein,‡ F. M. Pipkin, S. W. Raither, and L. K. Sisterson§

High Energy Physics Laboratory, Harvard University, Cambridge, Massachusetts 02138

(Received 1 October 1976)

We report measurements of kaon electroproduction from hydrogen and deuterium targets carried out at the Wilson Synchrotron Laboratory at Cornell University. The reactions $\gamma_V p \to K^+ X^0$, $K^+\Lambda$, and $K^+\Sigma^0$ were studied in the kinematic region $2.15 \leq W \leq 3.1$ GeV and $1.2 < Q^2 < 4.0$ GeV^2 as a function of Q^2, W, and ω. The $K^+\Sigma^0$ cross sections fall much more rapidly with increasing Q^2 than the $K^+\Lambda$ cross sections so that $K^+\Sigma^0/K\Lambda \to 0$ as Q^2 increases.

I. INTRODUCTION

Deep-inelastic electron scattering experiments have given important clues to the understanding of nucleon structure.[1] The cross section displays a remarkable regularity known as Bjorken scaling and is large compared to the cross section for elastic scattering. The nucleon behaves as if it were composed of pointlike constituents. By exploring the structure of the hadronic final state, one hopes to gain insight into the details of the interaction. Present knowledge of the final-state hadrons is based largely on data for production of pions and protons. The cross section for production of strange particles is much smaller and the available information on strange-particle production is still relatively sparse.

This paper reports measurements of K^+ meson electroproduction in the forward direction from hydrogen and deuterium targets. The experiment was carried out at the Wilson Synchrotron Laboratory at Cornell University. In addition to studying the inclusive K^+ meson production reaction

$$e+p \to e+K^++\text{anything}, \tag{1a}$$

we were able to resolve the specific channels

$$e+p \to e+K^++\Lambda, \tag{1b}$$

$$e+p \to e+K^++\Sigma^0, \tag{1c}$$

$$e+n \to e+K^++\Sigma^-. \tag{1d}$$

II. KINEMATICS

To first order in quantum electrodynamics, reactions (1a) through (1d) proceed via one-phonon exchange. The incident electron scatters and emits a virtual photon which subsequently interacts with the target nucleon. In effect, electroproduction is treated as photoproduction by a virtual photon whose mass squared $-Q^2$, energy ν, direction, and polarization parameter ϵ are tagged by the scattered electron. The electroproduction cross section is written as[2]

$$\frac{d\sigma(ep \to e'K^+X)}{d\Omega_{e'}dE'dp_{K^+}{}^3} = \Gamma \frac{d^3\sigma(\gamma_V p \to K^+X)}{dp_{K^+}{}^3}, \tag{2}$$

where

$$\Gamma = \frac{\alpha}{2\pi^2}\frac{E'}{E}\frac{W^2-M^2}{2MQ^2}\frac{1}{1-\epsilon}. \tag{3}$$

Here

$$\epsilon = \left[1+2\left(1+\frac{\nu^2}{Q^2}\right)\tan^2(\theta_{e'}/2)\right]^{-1}, \tag{4}$$

E is the laboratory energy of the incident electron, E' is the laboratory energy of the scattered electron, and W is the center-of-mass energy of the virtual-photon reaction.

It is conventional to describe the cross section for the reaction

$$\gamma_V N \to K^+X \tag{5}$$

in the center-of-mass frame, where the kaon variables are defined with respect to the virtual-photon direction. This cross section is a function of the virtual-photon variables Q^2, ν, and ϵ, the kaon variables θ^*, ϕ, and the missing mass M_X. Here θ^*, ϕ are the angular spherical coordinates of the kaon in the virtual-photon–target-nucleon center-of-mass system with the z axis taken as the direction of the virtual photon and the y axis perpendicular to the electron scattering plane. The cross section for reaction (5) is written

$$\frac{d\sigma}{d\Omega_K^* dM_X{}^2} = \frac{d\sigma_U}{d\Omega_K^* dM_X{}^2} + \epsilon\frac{d\sigma_L}{d\Omega_K^* dM_X{}^2} + \epsilon\frac{d\sigma_P}{d\Omega_K^* dM_X{}^2}\cos 2\phi + \left[\frac{\epsilon(\epsilon+1)}{2}\right]^{1/2}\frac{d\sigma_I}{d\Omega_K^* dM_X{}^2}\cos\phi. \tag{6}$$

The four terms arise respectively from unpolarized transverse photons, purely scalar photons, interference between the transverse amplitudes, and scalar-transverse interference. All the data reported in this paper have been averaged over ϕ

so that only the first two terms in Eq. (6) survive.

The inclusive virtual-photoproduction data can also be presented in terms of the Feynman[3] scaling variables x and $p_\perp^2$. Here $p_\perp$ is the transverse component of the kaon momentum and x is defined in terms of the center-of-mass momentum by the equation

$$x = p_\parallel^*/p_{\max}^*, \tag{7}$$

where $p_\parallel^*$ is the component of the kaon momentum along the virtual-photon direction and $p_{\max}^*$ is the maximum possible momentum as defined by the $K^+\Lambda$ final state.

For experiments at the comparatively low energies reported here, the variable x has the disadvantage that for x near 1 the range in $p_\perp^2$ is a function of x and W. To avoid this dependence we have chosen instead to use x', where

$$x' = p_\parallel^*/[(p_{\max}^*)^2 - p_\perp^2]^{1/2}. \tag{8}$$

The inclusive data have been analyzed in terms of the invariant structure function

$$F = \frac{E}{\sigma_{\text{tot}}}\frac{d^3\sigma}{dp_K^3} = \frac{1}{\sigma_{\text{tot}}}\frac{1}{\pi}\frac{E^*}{[(p_{\max}^*)^2 - p_\perp^2]^{1/2}}\frac{d\sigma}{dx'dp_\perp^2}. \tag{9}$$

Here σ_{tot} is the total virtual-photoproduction cross section for the W and Q^2 of the reaction. The value of σ_{tot} was taken from a fit to the electron scattering measurements of νW_2 with the assumption that $\sigma_S/\sigma_T = 0.18$.[4]

The virtual-photoproduction cross sections for the exclusive reactions (1b), (1c), and (1d) are expressed in the form $d\sigma/d\Omega^*$. These cross sections and the ratios of pairs of cross sections are studied as a function of Q^2, W, and the Bjorken scaling variable $\omega = 2M\nu/Q^2$.

III. EXPERIMENT

The apparatus consisted of two magnetic spectrometers set to either side of the incident electron beam as shown in Fig. 1. The focusing spectrometer located to the right of the beam was used to detect the scattered electrons. It consisted of two half quadrupoles, two bending magnets, and four x-y proportional wire-chamber planes. A low-pressure (17 psia) Freon-114 gas Čerenkov counter and a lead-Lucite shower counter were used to identify electrons. The spectrometer had a solid angle of 0.5 msr, a momentum resolution of 0.4% [full width at half maximum (FWHM)] for the central momentum, and a momentum acceptance of 50% (FWHM).

The spectrometer to the left of the beam detected the electroproduced K^+ meson. It consisted of a

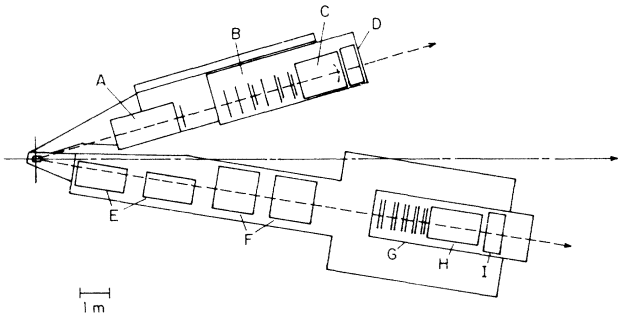

FIG. 1. A schematic diagram of the apparatus: A, 22D84 bending magnet; B, wire-chamber planes; C, Freon Čerenkov counter; D, lead-Lucite shower counter; E, 8Q48 half quadrupole magnets; F, 18D36 bending magnets; G, proportional wire chambers; H, Freon Čerenkov counter; I, lead-Lucite shower counter.

bending magnet, seven magnetostrictive x-y spark-chamber planes, a high-pressure (75 psia) Freon-12 gas Čerenkov counter, and a lead-Lucite shower counter. The trigger demanded that the K meson fire three scintillation counters which were located between chamber No. 4 and the Čerenkov counter. The time-of-flight difference between the electron and the kaon was recorded for each event. The spectrometer had a solid angle of 2.5 msr, a momentum resolution of 0.7% (FWHM), and a momentum acceptance of ±40%.

A Monte Carlo calculation assuming unit center-of-mass cross sections and incorporating multiple scattering, detector resolution, and geometrical effects was used to determine the acceptance. The normalization of the experiment was checked by independently observing elastically scattered electrons in each spectrometer and comparing the observed cross sections with the measured elastic-scattering cross section. The mean ratios of the measured elastic-scattering cross sections to the average of the world data for the electron and hadron arms were 0.994 ± 0.007 and 0.998 ± 0.009, respectively. The Monte Carlo program gave an angular resolution of roughly 0.3° (FWHM) in the center of mass and indicated that the resolution in angle and energy was multiple-scattering-limited.

Measurements were made at the points in the (Q^2, ν) plane shown in Fig. 2. At the circled points, both deuterium and hydrogen targets were used. The values of W and Q^2 shown in the figure are the central values. The acceptance of the apparatus was such that at each point the W distribution was roughly 0.9 GeV wide (FHWM) and the Q^2 distribution was 0.6 GeV^2 wide.

In the data analysis, the following procedure was used to separate K^+ mesons from pions and protons over the momentum range 0.5 to 4.6 GeV. Pions with momenta greater than 1.8 GeV/c were

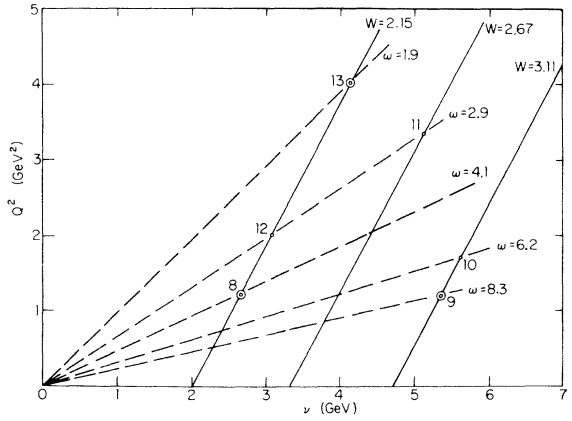

FIG. 2. The nominal values of Q^2 and W at which data were taken. The circles denote points at which data were taken with a deuterium target.

eliminated by rejecting all events in which the high-pressure Čerenkov counter fired. This cut did not affect the protons but it did eliminate kaons with momenta greater than 4.6 GeV/c. Time-of-flight cuts were used to analyze the remaining events. Figure 3 shows the cuts for kaons in the momentum interval from 2.2 to 3.2 GeV/c. The region marked "in-time kaons" extends from -0.9 nsec to 0.4 nsec, a point halfway between the kaon and proton timing peaks. From a study of pions, it was shown that the timing distribution is Gaussian with an rms resolution of 0.28 nsec. This result was used to correct for kaons lost through the upper timing cut. A correction for contamination due to protons and random events was made by subtracting the events in the region marked "random protons" from the "in-time kaons" data sample. For momenta less than 2.2 GeV/c, the kaon and proton timing peaks were sufficiently well separated that the proton contamination was negligible. Similar methods were used to separate kaons from pions for momenta smaller than 1.8 GeV/c.

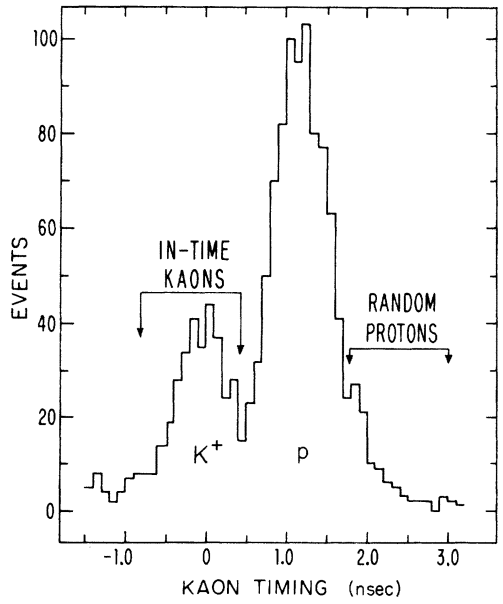

FIG. 3. The time-of-flight distribution for particles with momenta between 2.2 and 3.2 GeV/c at data point 9.

Momentum-independent corrections were made to the data for random coincidences [$(5 \pm 0.5)\%$], counter and spark-chamber dead time [$(5 \pm 2)\%$], absorption in the counters [$(2 \pm 1)\%$], target-wall background [$(5 \pm 3)\%$], chamber inefficiencies [$(1 \pm 0.5)\%$], and electron misidentification [$(2 \pm 0.5)\%$]. Momentum-dependent corrections arose from the timing cuts and the kaon decay in flight. The timing-cut correction ranged from $(19 \pm 2)\%$ at 4.6 GeV/c to 0 at 2.2 GeV/c for the kaon-proton separation region and from $(4 \pm 0.6)\%$ at 1.8 GeV/c to 0 at 1.3 GeV/c for the kaon-pion separation region. The decay-in-flight correction was the largest correction. It was calculated by a Monte Carlo program which simulated both the $K^+ \to \mu^+\nu$ and $K^+ \to \pi^+\pi^0$ decay modes in accordance with the known branching ratio. The correction for Monte Carlo events lost owing to geometry and kaon identification cuts ranged from $(200 \pm 4)\%$ at 1 GeV/c to $(30 \pm 1)\%$ at 4.6 GeV/c.

The quoted uncertainties are statistical only; there is an additional overall normalization uncertainty of 10% due principally to the uncertainty in the corrections.

IV. RESULTS

Figure 4 shows the invariant structure function for the inclusive K^+ reaction for $p_\perp^2 < 0.05$ GeV^2 at three values of Q^2 and two values of W. There is a peak at $x' = 1$ due to $K^+\Lambda$ production and a shoulder around $x' = 0.7$ which is possibly due to the $\Lambda(1520)$. The solid curve represents the π^+ invariant structure function for $p_\perp < 0.02$ GeV^2 multiplied by a scale factor of 0.2. Measurements reported earlier[5] show that the π^+ structure function is independent of Q^2 and varies by less than 20% over the region $2.0 < W < 3.2$ GeV. The K^+ invariant structure function above the resonance region behaves quite similarly, with no apparent W or Q^2 dependence in the kinematical range of this experiment. However, the K^+/π^+ ratio for $0.3 < x' < 0.7$ has more than doubled from a photoproduction value of $\simeq 0.1$ at $W = 3.5$ GeV (see Ref. 6) to 0.2–0.3 for our data with $1.2 < Q^2 < 4$ GeV^2 and $2.2 < W < 3.1$ GeV. The K^+ structure function appears less steep in its x' dependence than the π^+ structure function. Our restricted W range does not allow the production of

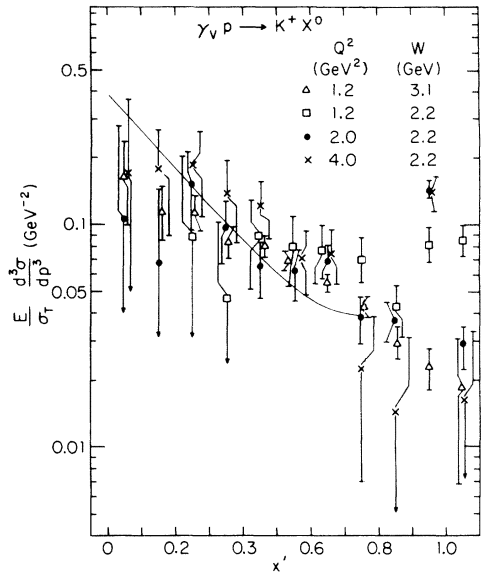

FIG. 4. The invariant structure functions for positive kaons with $p_\perp{}^2 < 0.05$ (GeV/c)^2 for data points 8, 9, 12, and 13. The solid curve is 0.20 times a fit (see Ref. 5) to the invariant structure function for inclusive production of positive pions with $p_\perp{}^2 < 0.02$ (GeV/c)^2.

more than one K^+ meson. The K^+ multiplicity is thus necessarily smaller than the π^+ multiplicity and could be the cause of the difference in the structure functions especially at low x'.

Figure 5 shows the cross section $d\sigma/d\Omega^* dM_X{}^2$ as a function of missing mass squared at the data point with $W = 2.2$ GeV and $Q^2 = 2.0$ GeV^2. There is a prominent peak corresponding to $K^+\Lambda$ production

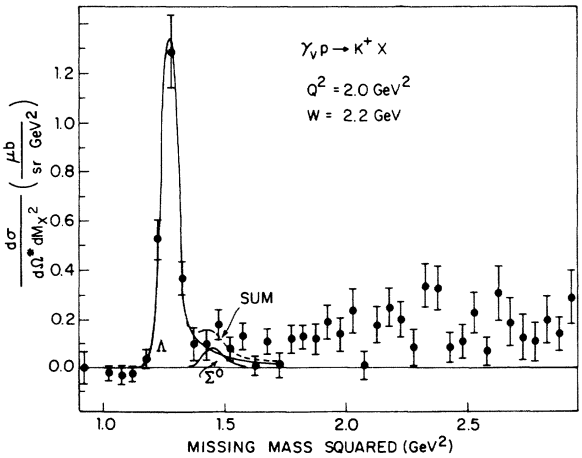

FIG. 5. Typical missing-mass spectrum for positive kaons together with the fits to the Λ and Σ^0 peaks used to determine the cross sections. For these data $\theta_K^* < 30°$.

and a smaller peak corresponding to $K^+\Sigma^0$ production. The Λ and Σ^0 cross sections were determined by fitting the missing-mass-squared distributions with curves constructed by folding Gaussian resolution functions with a radiative tail.[7,8] The solid line in Fig. 5 shows a typical fit to the data. The free parameters in the fit were the radiatively corrected Λ and Σ^0 cross sections and the central mass for the Λ peak. The difference in missing mass squared of the Λ and Σ^0 was constrained to its known value.

Table I summarizes the cross sections for the Λ and Σ^0 together with the average values of W, Q^2, ϵ, ω, and θ^*. The uncertainties in the graphs and tables include both statistical and fitting errors. The values of W and Q^2 at data points 9, 10, and 11 are shifted to lower W and higher Q^2 than the central values shown in Fig. 2 because of the 4.6-GeV/c momentum cutoff for the K^+.

Figure 6 shows a plot versus Q^2 of the Λ cross section for this experiment and earlier measurements by the CEA,[9] Harvard-Cornell,[10] and DESY[11] groups together with the result of a photoproduction experiment.[12] All data, except for the DESY measurements,[11] have been extrapolated to a common W by assuming that in the expression for the cross section

$$\frac{d\sigma}{d\Omega^*} = \frac{|\vec{p}_K^{\,*}|}{32\pi^2(W^2 - M^2)W} \times (\text{matrix element})^2 \quad (10)$$

the matrix element is not a function of W. Here $\vec{p}_K^{\,*}$ is the center-of-mass momentum of the detected kaon. The assumption that the matrix element is not a function of W is known experimentally to be correct for photoproduction,[13] where $(W^2 - M^2)^2 d\sigma/dt$ is found to be energy-independent and the expression corresponding to Eq. (10) is

$$\frac{d\sigma}{dt} = \left(\frac{1}{W^2 - M^2}\right)^2 \times (\text{matrix element})^2. \quad (11)$$

The agreement of the cross sections extrapolated from different values of W at $Q^2 = 1.2$ and 2.0 GeV^2 testifies to the validity of the extrapolation procedure. The DESY data[11] were extrapolated to $W = 2.15$ GeV using their measured W dependence, which, for values of $Q^2 \gtrsim 0.5$ GeV^2, agrees with our extrapolation procedure. The interpretation of the photoproduction point is subject to some uncertainty since it was taken at a fixed center-of-mass angle of $\theta^* = 25°$ while, except for the DESY electroproduction points[11] for which $\theta^* \leq 25°$, the electroproduction points are for data with $\theta^* < 15°$. If one takes the SLAC $d\sigma/dt$ photoproduction cross sections measured at higher energy[13] and uses the observed $(W^2 - M^2)^2$ dependence to extrapolate the low-t cross sections to $W = 2.15$ GeV, one obtains a value for $d\sigma/d\Omega^*$ which is the same as the value

TABLE I. A summary of the cross sections for the $K^+\Lambda$ and $K^+\Sigma^0$ channels for production from hydrogen in this experiment and the earlier CEA and Harvard-Cornell experiments.

Data point	θ^*_{bin} (deg)	Kinematic averages W (GeV)	Q^2 (GeV^2)	ϵ	ω	θ^* (deg)	$\frac{d\sigma}{d\Omega^*}(K^+\Lambda)$ $\left(\frac{\text{nb}}{\text{sr}}\right)$	$\frac{d\sigma}{d\Omega^*}(K^+\Sigma^0)$ $\left(\frac{\text{nb}}{\text{sr}}\right)$	$\frac{d\sigma}{d\Omega^*}(K^+\Sigma^0)\Big/\frac{d\sigma}{d\Omega^*}(K^+\Lambda)$	$\frac{d\sigma}{d\Omega^*}(K^+\Lambda)\Big/\frac{d\sigma}{d\Omega^*}(\pi^+ n)$	Extrapolated to 2.15 GeV $\frac{d\sigma}{d\Omega^*}(K^+\Lambda)$ $\left(\frac{\text{nb}}{\text{sr}}\right)$	Extrapolated to 2.15 GeV $\frac{d\sigma}{d\Omega^*}(K^+\Sigma)$ $\left(\frac{\text{nb}}{\text{sr}}\right)$
							Data from present experiment					
8	<15	2.17	1.18	0.94	4.25	8.0	251±43	73±30	0.29±0.13	0.075±0.013	254±44	73±30
8	<30	2.22	1.18	0.94	4.44	11.0	203±32	52±22	0.26±0.12	0.092±0.015	211±33	54±22
12	<15	2.15	1.98	0.94	2.92	9.1	193±22	17±12	0.09±0.06	0.125±0.016	193±22	17±12
12	<30	2.20	1.95	0.94	3.10	13.9	176±13	10±6	0.06±0.03	0.153±0.013	181±13	10±6
13	<15	2.17	3.98	0.88	1.98	9.0	78±15	10±10	0.13±0.13	0.165±0.036	79±15	10±10
13	<30	2.21	3.92	0.87	2.05	14.0	64±7	7±5	0.11±0.08	0.167±0.020	66±7	7±7
9	<15	2.85	1.36	0.87	6.30	10.4	142±31	24±25	0.17±0.18	0.085±0.026	216±47	35±36
9	<30	2.71	1.41	0.88	5.63	16.3	120±17	36±15	0.30±0.13	0.103±0.015	169±24	49±20
11	<15	2.51	3.46	0.85	2.55	10.0	97±29	5±8	0.05±0.09	0.179±0.056	120±36	6±10
11	<30	2.42	3.57	0.86	2.30	14.8	67±15	6±6	0.09±0.09	0.151±0.035	72±18	7±7
10	<30	2.66	2.04	0.88	3.98	19.2	92±25	7±14	0.08±0.16	0.114±0.031	125±34	9±19
							Harvard-Cornell data					
1	<15	2.67	0.62	0.86	11.08	7.8	267±26	35±15	0.13±0.07	0.064±0.006	365±35	46±20
2–4	<15	2.66	1.20	0.86	6.14	8.4	169±12	38±8	0.23±0.06	0.070±0.005	229±17	50±10
7	<15	2.66	2.00	0.82	4.11	7.5	137±13	6±6	0.04±0.05	0.113±0.011	185±17	8±8
6	<15	2.20	1.18	0.94	4.15	7.4	272±19	35±12	0.13±0.05	0.083±0.006	279±20	36±12
							CEA data					
	<15	2.17	0.18	0.85	22.8	5.9	553±84	<53	<0.10	0.116±0.028	539±85	
	<15	2.17	0.29	0.88	14.0	5.9	499±57	94±48	0.21±0.11	0.085±0.020	454±58	95±48
	<15	2.17	0.40	0.86	10.7	5.9	398±46	60±40	0.15±0.10	0.069±0.015	402±47	60±40
	<15	2.17	0.76	0.81	5.8	5.9	287±42	75±33	0.26±0.12	0.064±0.016	290±42	75±33
	<15	2.17	1.17	0.78	4.2	5.9	277±45	<42	<0.15	0.122±0.025	280±45	
	<15	1.93	0.29	0.93	10.8	6.0	732±14	336±147	0.46±0.22	0.096±0.026	676±129	329±144
	<15	2.10	0.29	0.90	13.2	6.0	369±90	192±84	0.52±0.26	0.061±0.019	360±88	189±83
	<15	2.48	0.29	0.74	19.2	6.0	350±33	123±29	0.35±0.09	0.104±0.022	425±40	145±34

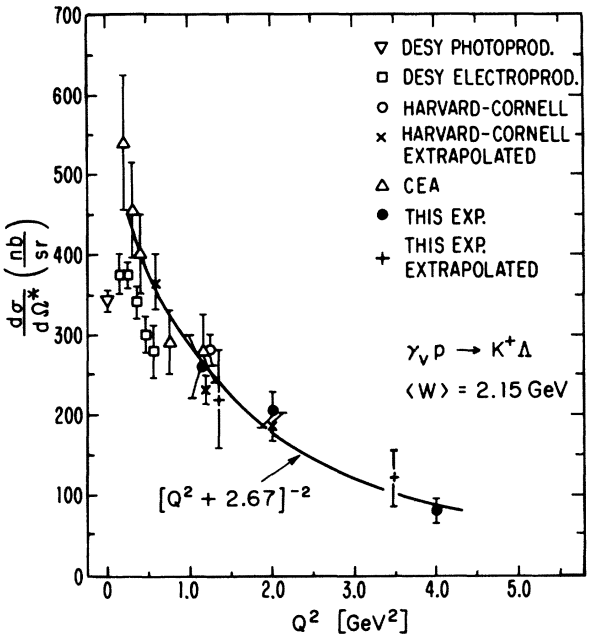

FIG. 6. The Q^2 dependence of the $K^+\Lambda$ cross section using data with $\theta^* < 15°$ from this experiment and the earlier CEA (see Ref. 9) and Harvard-Cornell (see Ref. 10) measurements. Some of the data have been extrapolated to a common W with the assumption that the W dependence is given by $|p_K^*|/[(W^2 - M^2)W]$. Also shown are DESY electroproduction data (see Ref. 11) with $\theta^* \lesssim 25°$ and DESY photoproduction data (see Ref. 12) with $\theta^* = 25°$. The solid curve gives a fit to all data with $\theta^* < 15°$.

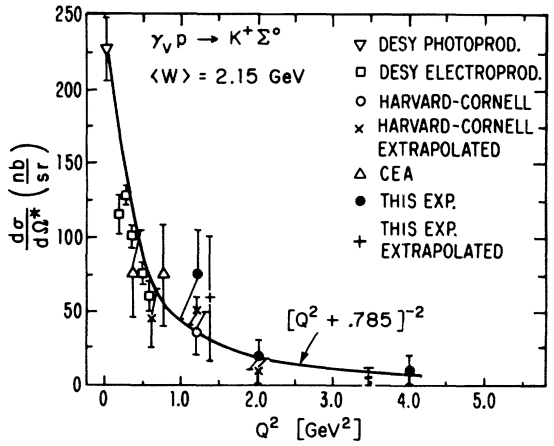

FIG. 7. The Q^2 dependence of the $K^+\Sigma^0$ cross section using data with $\theta^* < 15°$ from this experiment and the earlier CEA (see Ref. 9) and Harvard-Cornell measurements (see Ref. 10). Some of the data have been extrapolated to a common W with the assumption that the W dependence is given by $|p_K^*|/[(W^2 - M^2)W]$. Also shown are DESY electroproduction data (see Ref. 11) with $\theta^* \lesssim 25°$ and DESY photoproduction data (see Ref. 12) with $\theta^* = 25°$. The solid curve gives a fit to all data with $\theta^* < 15°$.

reported by Feller *et al.*[12] at $|t| = 0.147$ GeV^2. A cross section that initially rises with Q^2 indicates that both scalar and transverse photons contribute to the reaction. In the absence of scalar-photon contributions, the cross section is expected to decline monotonically with increasing Q^2. The uncertainty of the photoproduction point leaves this matter unresolved. A fit of the Q^2 dependence of the CEA and Harvard-Cornell data to the form $(Q^2 + M^2)^{-2}$ gives $M^2 = (2.67 \pm 0.28)$ GeV^2.

Figure 7 shows the energy-extrapolated Σ^0 cross sections as a function of Q^2. The procedure followed was identical to the one used to project the $K^+\Lambda$ cross section to a common W. The $K^+\Sigma^0$ cross section drops rapidly from the value observed in photoproduction as Q^2 increases. A fit of the CEA and Harvard-Cornell data to the form $(Q^2 + M^2)^{-2}$ gives $M^2 = (0.785 \pm 0.095)$ GeV^2. This fit is shown as a solid line in Fig. 7.

Figures 8(a) and 8(b) show the Σ^0/Λ ratio as a function of $1/\omega$ and Q^2, respectively. The ratio decreases rapidly as Q^2 or $1/\omega$ increases.

Table II summarizes the $\gamma_v n \rightarrow K^+\Sigma^-$ cross sections determined from an analysis of the deuterium data. The procedure used to analyze the deuterium data was the same as that used with the hydrogen data. The $\gamma_v n \rightarrow K^+\Sigma^-$ cross section was then calculated with the assumption that the deuterium cross section was equal to the sum of the cross sections for the proton and the neutron.

V. DISCUSSION

An increase of the electroproduction data for $K^+\Lambda$ from the photoproduction cross section to a peak at low Q^2 suggests a large scalar contribution due to one-kaon exchange analogous to that in the $\pi^+ n$ channel.[14,15] A large one-kaon-exchange contribution used in conjunction with the fact that $g_{K\Lambda N} \gg g_{K\Sigma^0 N}$ would also explain the small $K^+\Sigma^0/K^+\Lambda$ ratio observed in electroproduction. Bartl and Majerotto[16] argue that such a model is not tenable and that it leads to serious difficulties in understanding the photoproduction cross section.

Two attempts of intermediate sophistication have been carried out to construct a theory of kaon electroproduction. Levy, Majerotto, and Read[17,18] extrapolated an absorbed Regge model with K and K^*-K^{**} exchange-degenerate trajectories which describes kaon photoproduction quite well in the most straightforward way to the region of spacelike photon mass without introducing any new parameters. The theoretical predictions turned out to be too small by a factor of 2 when compared with measured values reported by the DESY group.

More recently, Bartl and Majerotto[16] added to this model an unnatural-parity contribution arising

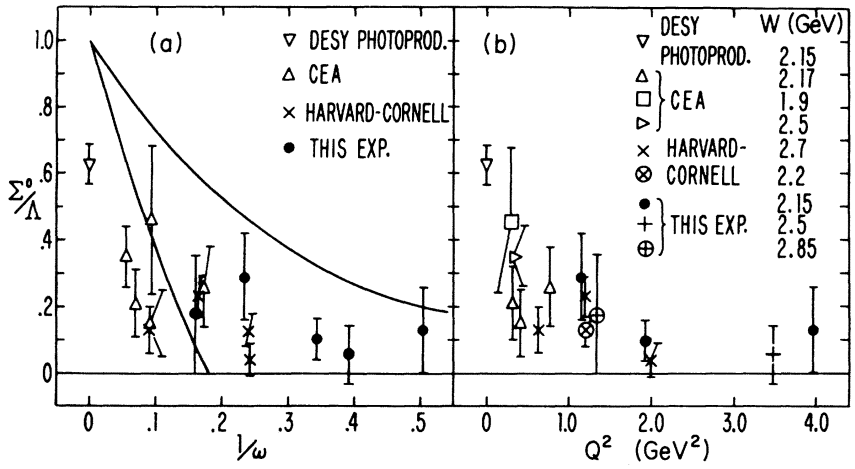

FIG. 8. (a) A plot of the ratio of the cross sections for the $K^+\Sigma^0$ and $K^+\Lambda$ channels as a function of $1/\omega$ for data with $\theta^* < 15°$. The solid curves are the upper and lower limits of a parton-model analysis due to Nachtmann (see Ref. 20). (b) A plot of the ratio of the cross sections for the $K^+\Sigma^0$ and $K^+\Lambda$ channels as a function of Q^2 for data with $\theta^* < 15°$.

from $K_B(1^{+-})$ or $K_A(1^{++})$. They were able to fit DESY data at $W = 2.24$ GeV with either hypothesis. The first calculation used $K_B(1^{+-})$ with strict exchange degeneracy between K and K_B for $Q^2 = 0$ and broken exchange degeneracy for $Q^2 > 0$. The second model maintained strict exchange degeneracy for both K^*-K^{**} and K-K_B and introduced the contribution of a $K_A(1^{++})$-$K_A(2^{--})$ exchange-degenerate trajectory. Neither of these models gives a good fit to the Harvard-Cornell data at $W = 2.66$ GeV. This indicates that the theory does not give the correct energy dependence.

There are several ways in which one can understand the decrease in the Σ^0/Λ ratio as Q^2 increases. Parton-model calculations, based on the inelastic-electron-scattering measurements which show that $\nu W_2^n/\nu W_2^p$ appears to approach $\frac{1}{4}$ as $\omega \to 1$, predict that $\Sigma^0/\Lambda \to 0$ as $\omega \to 1$.[19-21] In its most naive form the argument is made that in the limit $\omega \to 1$ mainly p quarks are being projected out of the proton, leaving behind an isospin-zero core. When a kaon is then produced in the near forward direction, the production of accompanying $I = 1$ baryons is greatly disfavored compared to the production of $I = 0$ baryons. The solid curves in Fig. 8(a) are the upper and lower limits predicted by Nachtmann[20] from a more sophisticated quark-model analysis. The data for $\omega < 6$ lie within the predicted limits.

Cleymans and Close[21] have carried out a more general analysis of the exclusive kaon reactions in the limit $\omega \to 1$ from both the standpoint of the quark model and more general SU(3) considerations. Utilizing the fact that $\nu W_2^n/\nu W_2^p \to \frac{1}{4}$ as $\omega \to 1$, they conclude that either model predicts that as $\omega \to 1$, $K^+\Sigma/K^+\Lambda \to 0$, and with the assumption that $F = D$, $K^+\Lambda/\pi^+ n \to \frac{2}{3}$. Figure 9 shows the measured ratio of the cross sections for $K^+\Lambda$ and $\pi^+ n$ for $\theta^* < 15°$ as a function of $1/\omega$ and Q^2. The solid curves are those predicted by both the quark model and SU(3) when it is assumed there is no coupling to the decuplet states.

TABLE II. A summary of the cross sections for the $K^+\Sigma$ channel determined from deuterium data.

Data point	Kinematic averages θ^*_{bin} (deg)	W (GeV)	Q^2 (GeV^2)	ϵ	θ^* (deg)	$\frac{d\sigma}{d\Omega^*}(K^+\Sigma)\Big\|_{D_2}\Big/\frac{d\sigma}{d\Omega^*}(K^+\Sigma^0)\Big\|_{H_2}$	$\frac{d\sigma}{d\Omega^*}(K^+\Sigma^0)\Big\|_p$ (nb/sr)	$\frac{d\sigma}{d\Omega^*}(K^+\Sigma^-)\Big\|_n$ (nb/sr)
9	$\theta < 15$	2.83	1.29	0.88	10.6	1.60±1.40	40±29	14±34
9	$\theta < 30$	2.71	1.35	0.89	15.8	1.70±0.80	36±15	25±29
8	$\theta < 15$	2.16	1.20	0.94	8.4	1.76±0.86	73±30	55±63
8	$\theta < 30$	2.21	1.19	0.94	11.5	2.80±1.25	52±22	94±65
13	$\theta < 15$	2.15	3.97	0.88	8.2	1.20±2.51	10±10	2±25
13	$\theta < 30$	2.28	3.84	0.87	15.4	3.00±2.71	7±5	14±19

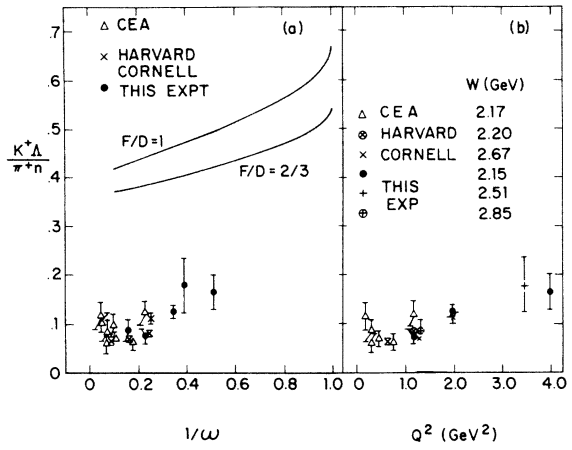

FIG. 9. (a) A plot versus $1/\omega$ of the ratio of the cross sections for the $K^+\Lambda$ and $\pi^+ n$ channels for $\theta^* < 15°$. The solid curves are the predictions of a simple SU(3) model which assumes no coupling to the decuplet. The upper curve is given by a simple parton-model calculation which assumes no coupling to the decuplet. (b) A plot versus Q^2 of the ratio of the cross sections for the $K^+\Lambda$ and $\pi^+ n$ channels for $\theta^* < 15°$.

VI. CONCLUSIONS

The $K^+\Sigma^0$ cross section decreases rapidly and monotonically with increasing Q^2. This behavior suggests the absence of a large contribution by scalar photons. While the $K^+\Lambda$ measurements do not exclude a sizable scalar-photon contribution, a detailed analysis is made difficult by the difference in the center-of-mass angles at which the photoproduction and electroproduction data were taken. The $K^+\Sigma^0/K^+\Lambda$ ratio decreases as Q^2 increases, a fact that can be understood by both simple SU(3) and the parton model. The results for the inclusive K^+ reaction indicate that there are no dramatic changes as the photon becomes massive.

ACKNOWLEDGMENTS

We wish to acknowledge the support of Professor Boyce McDaniel, the staff of the Wilson Synchrotron Laboratory, and the staff of the Harvard Cyclotron Laboratory. We would like to thank the Electron Scattering Group at Cornell for the use of their spectrometer.

*Research supported in part by ERDA under Contract No. AT(11-1)-3064.

†Present address: Fermi National Accelerator Laboratory, P. O. Box 500, Batavia, Illinois 60510.

‡Present address: P. O. Box 29246, Los Angeles, California 90029.

§Present address: 36 Webb St., Lexington, Massachusetts 02173.

[1]R. P. Feynman, *Photon-Hadron Interactions* (Benjamin, Reading, Mass., 1972).

[2]L. N. Hand, Phys. Rev. 129, 1834 (1963).

[3]R. P. Feynman, Phys. Rev. Lett. 23, 1415 (1969).

[4]W. B. Atwood (private communication).

[5]C. J. Bebek, C. N. Brown, M. Herzlinger, S. D. Holmes, C. A. Lichtenstein, F. M. Pipkin, S. Raither, and L. K. Sisterson, Phys. Rev. Lett. 34, 759 (1975).

[6]H. Burfeindt, G. Buschhorn, H. Genzel, P. Heide, U. Kotz, K. H. Mess, P. Schmuser, B. Sonne, G. Vogel, and B. M. Wiik, Nucl. Phys. B74, 189 (1974).

[7]L. W. Mo and Y.-S. Tsai, Rev. Mod. Phys. 41, 205 (1969).

[8]A. Bartl and P. Urban, Acta Phys. Austriaca 24, 139 (1966).

[9]C. N. Brown, C. R. Canizares, W. E. Cooper, A. M. Eisner, G. J. Feldman, C. A. Lichtenstein, L. Litt, W. Lockeretz, W. B. Montana, F. M. Pipkin, and N. Hicks, Phys. Rev. Lett. 28, 1086 (1972).

[10]C. J. Bebek, C. N. Brown, M. Herzlinger, S. Holmes, C. A. Lichtenstein, F. M. Pipkin, L. K. Sisterson, D. Andrews, K. Berkelman, D. G. Cassel, D. L. Hartill, and N. Hicks, Phys. Rev. Lett. 32, 21 (1974).

[11]T. Azemoon, I. Dammann, C. Driver, D. Lüke, G. Specht, K. Heinloth, H. Ackermann, E. Ganssauge, F. Janata, and D. Schmidt, Nucl. Phys. B95, 77 (1975).

[12]P. Feller, D. Menze, U. Opara, W. Schulz, and W. J. Schwille, Nucl. Phys. B39, 413 (1972).

[13]A. M. Boyarski, F. Bulos, W. Busza, R. Diebold, S. D. Ecklund, G. E. Fischer, Y. Murata, J. R. Rees, B. Richter, and W. S. C. Williams, Phys. Rev. Lett. 22, 1131 (1969).

[14]C. N. Brown, C. R. Canizares, W. E. Cooper, A. M. Eisner, G. J. Feldman, C. A. Lichtenstein, L. Litt, W. Lockeretz, V. B. Montana, and F. M. Pipkin, Phys. Rev. D 8, 92 (1973).

[15]C. J. Bebek, C. N. Brown, M. Herzlinger, S. Holmes, C. A. Lichtenstein, F. M. Pipkin, L. K. Sisterson, D. Andrews, K. Berkelman, D. G. Cassel, and D. L. Hartill, Phys. Rev. D 9, 1229 (1974).

[16]A. Bartl and W. Majerotto, Nucl. Phys. B90, 285 (1975).

[17]N. Levy, W. Majerotto, and B. J. Read, Nucl. Phys. B55, 493 (1973).

[18]N. Levy, W. Majerotto, and B. J. Read, Nucl. Phys. B55, 513 (1973).

[19]F. E. Close, Nucl. Phys. B73, 410 (1974).

[20]O. Nachtmann, Nucl. Phys. B74, 422 (1974).

[21]J. Cleymans and F. E. Close, Nucl. Phys. B85, 429 (1975).